1290 *Biochemistry* **2010,** *49,* 1290–1296
DOI: 10.1021/bi9020296

BIOCHEMISTRY
including biophysical chemistry & molecular biology
Article

Effects of Interdomain Tether Length and Flexibility on the Kinetics of Intramolecular Electron Transfer in Human Sulfite Oxidase[†]

Kayunta Johnson-Winters, Anna R. Nordstrom, Safia Emesh, Andrei V. Astashkin, Asha Rajapakshe, Robert E. Berry, Gordon Tollin,* and John H. Enemark*

Department of Chemistry and Biochemistry, The University of Arizona, Tucson, Arizona 85721

Received November 25, 2009; Revised Manuscript Received January 8, 2010

ABSTRACT: Sulfite oxidase (SO) is a vitally important molybdenum enzyme that catalyzes the oxidation of toxic sulfite to sulfate. The proposed catalytic mechanism of vertebrate SO involves two intramolecular one-electron transfer (IET) steps from the molybdenum cofactor to the iron of the integral *b*-type heme and two intermolecular one-electron steps to exogenous cytochrome *c*. In the crystal structure of chicken SO [Kisker, C., et al. (1997) *Cell 91*, 973−983], which is highly homologous to human SO (HSO), the heme iron and molybdenum centers are separated by 32 Å and the domains containing these centers are linked by a flexible polypeptide tether. Conformational changes that bring these two centers into greater proximity have been proposed [Feng, C., et al. (2003) *Biochemistry 42*, 5816−5821] to explain the relatively rapid IET kinetics, which are much faster than those theoretically predicted from the crystal structure. To explore the proposed role(s) of the tether in facilitating this conformational change, we altered both its length and flexibility in HSO by site-specific mutagenesis, and the reactivities of the resulting variants have been studied using laser flash photolysis and steady-state kinetics assays. Increasing the flexibility of the tether by mutating several conserved proline residues to alanines did not produce a discernible systematic trend in the kinetic parameters, although mutation of one residue (P105) to alanine produced a 3-fold decrease in the IET rate constant. Deletions of nonconserved amino acids in the 14-residue tether, thereby shortening its length, resulted in more drastically reduced IET rate constants. Thus, the deletion of five amino acid residues decreased IET by 70-fold, so that it was rate-limiting in the overall reaction. The steady-state kinetic parameters were also significantly affected by these mutations, with the P111A mutation causing a 5-fold increase in the sulfite K_m value, perhaps reflecting a decrease in the ability to bind sulfite. The electron paramagnetic resonance spectra of these proline to alanine and deletion mutants are identical to those of wild-type HSO, indicating no significant change in the Mo active site geometry.

Sulfite oxidase (SO)[1] catalyzes the oxidation of sulfite to sulfate, using oxidized ferricytochrome *c* (cyt c_{ox}) as the physiological electron acceptor (eq 1) (*1*−*4*). This reaction is biologically essential, serving as the final step in the catabolism of sulfur-containing amino acids, methionine and cysteine, and as a detoxification mechanism for sulfite.

$$SO_3^{2-} + H_2O + 2(\text{cyt } c)_{ox} \rightarrow SO_4^{2-} + 2(\text{cyt } c)_{red} + 2H^+ \quad (1)$$

In animals, SO is located in the mitochondrial intermembrane space (*5*, *6*), and the kinetics of chicken (*7*−*9*), rat (*10*), and human SO (*11*−*15*) have been extensively studied. The only crystal structure for an intact animal SO is that of the chicken liver enzyme (*16*). The structure confirms that the protein is a homodimer. Each ∼51.5 kDa subunit contains a b_5-type cytochrome heme domain (∼10 kDa) at the N-terminus. The larger C-terminal domain contains the molybdopterin cofactor (Moco). These two domains are bridged by a flexible polypeptide tether (Figure 1) which is poorly resolved in the crystal structure (*16*). The distance between the Mo and Fe atoms in the crystal conformation is 32 Å, but the apparent disorder of the tether suggests that it has high flexibility and may mediate conformational changes that alter the distance between the Fe and Mo centers (*17*).

The proposed catalytic mechanism of vertebrate SO involves two intramolecular one-electron transfer (IET) steps from the molybdenum cofactor to the heme iron, and two intermolecular one-electron steps to exogenous cytochrome *c* (cyt *c*) (*1*). Extensive investigations of the IET kinetics in cSO (*7*−*9*) and HSO (*11*−*15*) using laser flash photolysis have been reported. The observed IET rates are much faster than expected for electron tunneling processes (*18*, *19*) on the basis of previous studies of electron tunneling kinetics in model systems and in proteins (*19*−*43*). For example, Gray and co-workers have correlated intramolecular electron tunneling rates with the donor−acceptor distance in protein solutions and structurally characterized crystals for more than 30 metalloproteins with a wide range of thermodynamic driving force (i.e., redox potential differences) (*32*, *36*). However, if these tunneling time scales are

[†]This research was supported by National Institutes of Health (NIH) Grant GM-037773 (to J.H.E.) and Ruth L. Kirchstein-NIH Fellowship 1F32GM082136-01 (to K.J.-W.).

*To whom correspondence should be addressed. J.H.E.: e-mail, jenemark@u.arizona.edu; phone, (520) 621-2245; fax, (520) 626-8065. G.T.: e-mail, gtollin@u.arizona.edu; phone, (520) 621-3447; fax, (520) 621-9288.

[1]Abbreviations: SO, sulfite oxidase; dRF, 5-deazariboflavin; cSO, chicken sulfite oxidase; HSO, human sulfite oxidase; cyt *c*, cytochrome *c*; IET, intramolecular electron transfer; k_{et}, electron transfer rate constant; K_{eq}, equilibrium constant for intramolecular electron transfer; k_f and k_r, microscopic rate constants for the forward and reverse directions, respectively, of intramolecular electron transfer; Moco, molybdopterin cofactor; *wt*, wild type.

 Published on Web 01/11/2010

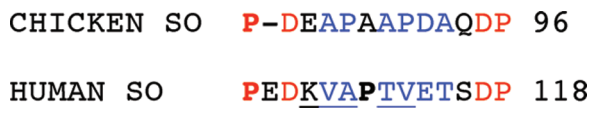

FIGURE 1: Sequence alignment of the flexible tether regions of cSO and HSO. Amino acids highlighted in red are conserved between the two species, while those highlighted in blue are similar. Mutations discussed in this work are indicated in the HSO sequence: proline residues mutated to alanines are in bold type, and deleted residues are underlined.

applied to the crystal structure of cSO, then IET through the 32 Å distance between the Mo and Fe centers should proceed on a time scale of seconds, rather than the millisecond times that are found experimentally (*17*, *44*). Thus, the results for SO imply that the distance between the Fe and Mo centers during IET is much less than the 32 Å separation found in the crystal structure (*16*).

Feng et al. (*17*) showed that the IET rate constant in cSO decreased with increasing solvent viscosity. They proposed that interdomain motion that decreases the Mo−Fe distance is essential for rapid IET and that the flexible tether linking the two domains of SO facilitates this motion. Steady-state kinetics and electron paramagnetic resonance (EPR) measurements with SO were also consistent with this hypothesis (*17*).

Kawatsu and Beratan have used a computational model to explore the mechanisms of IET in proteins such as SO, where domains containing two cofactors are linked by a flexible tether (*45*). They found that the constrained conformational flexibility of the tether introduces an entropic component to the effective donor−acceptor interaction potential that produces a kinetic regime intermediate between "unimolecular" and "bimolecular". Their calculations predicted that for SO the tether length may control the transition between the electron tunneling and diffusion-limited regimes.

Figure 1 shows the tether sequences for chicken and human SO. To date, there have been no investigations of the role of specific amino acids in the tether on the reactivity and spectroscopic properties of SO. Here, we have used mutagenesis of the tether of HSO to increase its conformational flexibility (P105A and P111A) and to decrease its length (deletion of the nonconserved amino acids, K108, V109, A110, T112, and V113). The effects of these modifications of the tether on the IET and steady-state kinetics, as well as on the EPR spectra of HSO, are described below.

MATERIALS AND METHODS

Site-Directed Mutagenesis. Expression plasmids of HSO mutants were constructed using the pTG918 plasmid via the Quick Change site-directed mutagenesis protocol (Stratagene), and the primers are listed in Table S1 of the Supporting Information. The mutations were verified by sequence analysis performed at the Sequetech Corp. DNA Analysis facility (Mountain View, CA). Recombinant ΔK108V109A110 (ΔKVA), ΔK108V109A110T112 (ΔKVAT), and ΔK108V109A110T112V113 (ΔKVATV) HSO are mutant proteins in which the specific amino acids named were deleted from the tether.

Protein Overexpression and Purification. Recombinant P105A, P111A, and P105A/P111A and ΔKVA, ΔKVAT, and ΔKVATV deletion HSO mutants were purified as previously described (*46*, *47*) with the following modifications. After the Phenyl Sepharose column (GE Healthcare), fractions exhibiting an A_{413}/A_{280} ratio of ≥0.80 were pooled and further purified using a Superdex 200 column (GE Healthcare). Fractions exhibiting an A_{413}/A_{280} ratio of ≥0.96 were then pooled and used in the experiments described in this study. The molybdenum content of purified SO proteins was determined using an IRIS Advantage Inductively Coupled Plasma Emission Spectrometer from the Jarrell Ash Corp. (see the Supporting Information). Enzyme concentrations were determined by using a molar extinction coefficient of 113000 M^{-1} cm^{-1} at 413 nm for oxidized human SO (*14*).

Laser Flash Photolysis. Laser flash photolysis experiments were performed anaerobically on 0.30 mL solutions containing ~90 μM 5-deazariboflavin (dRF) and 0.5 mM freshly prepared semicarbazide as a sacrificial reductant. The methodologies used to obtain rate and equilibrium constants for IET in SO have been described previously (*48*) and are summarized below. The laser flash photolysis apparatus system has been extensively described (*49*), as has been the basic photochemical process by which 5-deazariboflavin semiquinone (dRFH$^\bullet$) is generated by reaction between triplet-state dRF and the sacrificial reductant and used to reduce redox-active proteins (eqs 2−5) (*50*−*52*).

$$\mathrm{dRF} \rightarrow {}^1\mathrm{dRF} \rightarrow {}^3\mathrm{dRF} \tag{2}$$

$${}^3\mathrm{dRF} + \mathrm{AH_2} \rightarrow \mathrm{dRFH^\bullet} + \mathrm{AH^\bullet} \tag{3}$$

$$\mathrm{dRFH^\bullet} + \mathrm{Mo(VI)/Fe(III)} \rightarrow \mathrm{dRF} + \mathrm{Mo(VI)/Fe(II)} \tag{4}$$

$$\mathrm{Mo(VI)/Fe(II)} \underset{k_r}{\overset{k_f}{\rightleftharpoons}} \mathrm{Mo(V)/Fe(III)} \tag{5}$$

The IET rate constant can be calculated by fitting the heme reoxidation curve with an exponential function (eq 6) where the IET rate constant is the sum of the forward and the reverse electron transfer rate constants (k_f and k_r, respectively, in eq 7).

$$\frac{\mathrm{d}A_{553}}{\mathrm{d}t} = a + b\exp(-k_{et}t) \tag{6}$$

$$k_{et} = k_f + k_r \tag{7}$$

The equilibrium constant can then be calculated using the parameters a and b, which are determined from the kinetic traces. A_0 is the absorbance extrapolated to time zero, assuming that the photochemically induced reduction of SO is instantaneous.

$$a = A_0\frac{k_r}{k_{et}} = A_0\frac{k_r}{k_f + k_r} \tag{8}$$

$$b = A_0\frac{k_f}{k_{et}} = A_0\frac{k_f}{k_f + k_r} \tag{9}$$

$$K_{eq} = \frac{k_f}{k_r} = \frac{b}{a} \tag{10}$$

The forward and reverse rate constants (k_f and k_r, respectively) of IET can then be calculated from the equilibrium constant (eq 10), thereby providing quantitative information about interdomain electron transfer in the enzyme. Note that k_f in these flash photolysis experiments is actually the reverse of the net physiological IET direction.

Steady-State Assays. Steady-state kinetic studies were performed aerobically in a Varian Cary-300 spectrophotometer. Initial velocities were determined by following the reduction of a

freshly prepared oxidized cyt *c* (horse heart, Sigma) solution at 550 nm, using an extinction coefficient change of 19630 M^{-1} cm^{-1} (*8*). SO was routinely assayed at 25 °C in 20 mM Tris (pH 8.0), titrated with acetic acid. We conducted the steady-state kinetic pH profile study by using a saturating concentration of cyt *c*, 400 μM (10-fold greater than K_m), and varying the concentration of sulfite, between 2 and 200 μM. Also, the steady-state kinetic profile for obtaining the K_m for cyt *c* was studied using saturating concentrations of sulfite, with the cyt *c* concentration varying between 3 and 200 μM.

Spectroelectrochemistry. Wild type (*wt*) HSO and ΔKV-ATV HSO were used at enzyme concentrations ranging from 350 to 370 μM. Methods for spectroelectrochemical measurements of the heme reduction potential utilized the same instrumentation and the same type of reference electrode [Ag/AgCl, $E_m = -205$ mV vs the standard hydrogen electrode (SHE)] as described previously (*53*, *54*). Protein solutions for electrochemical studies were prepared in 100 mM phosphate buffer (pH 7.5) containing 15 electrochemical mediators selected to cover a wide potential titration range: *N*,*N*-dimethyl-1,4-phenylenediamine, *N*,*N*-diethyl-2-methyl-1,4-phenylenediamine, 1,1′-dimethylferrocene, tetrachlorobenzoquinone, tetramethyl-*p*-phenylenediamine, 2,6-dichlorophenolindophenol, 1,2-naphthoquinone, trimethylhydroquinone, hexaammineruthenium chloride, 2-methyl-1,4-naphthalenedione, 2-hydroxy-1,4-naphthoquinone, anthraquinone 2-sulfonate, neutral red, benzyl viologen, and methyl viologen each at 40 μM (all purchased from Aldrich) (*55*). To minimize the final sample volume used in each experiment, we filled the void volume between the reference electrode and the optical window with 100 mM phosphate buffer (pH 7.5) containing 5% high-strength agarose (Bio-Rad). Since the ratio of oxidized to reduced forms of each redox species is directly related to the absorbances of the optical spectra via Beer's law (assuming the extinction coefficients of the reduced and oxidized species are different at the chosen wavelength), the change in absorbance with respect to applied potential can be fit to the Nernst equation (eq 11) using the nonlinear least-squares fitting algorithm in Origin.

$$E_{app} = E^0 + 2.303(RT/nF)\log_{10}([Ox]/[Red]) \qquad (11)$$

where E_{app} is the applied potential, E^0 is the midpoint potential determined from these data, and [Ox] and [Red] are the concentrations of the Fe(III) and Fe(II) states of the b_5 heme of HSO, respectively.

Mo EPR Spectroscopy Experiments. EPR samples of *wt*, ΔKVA, ΔKVAT, and ΔKVATV (0.5−0.7 mM HSO) at pH 5.8 were prepared in 100 mM Bis-Tris buffer containing 100 mM NaCl (*56*−*59*). For high-pH (pH 9.0) samples, 100 mM Bis-Tris propane buffer was employed. The enzyme samples were reduced with a 20-fold excess of sodium sulfite and immediately frozen in liquid nitrogen. The continuous wave (CW) X-band EPR spectra were recorded on a Bruker ESP-300 spectrometer at 77 K.

RESULTS AND DISCUSSION

Laser Flash Photolysis Kinetics of Proline to Alanine Mutants. The tether of cSO has a sequence very different from that of HSO (Figure 1). Furthermore, previous laser flash photolysis studies have shown that cSO has an IET rate constant (k_{et}) twice that of HSO (*11*). This result could be due to the greater flexibility of the tether in cSO, which has four alanine residues compared to one for HSO (although cSO has one more proline residue). To test this hypothesis, we mutated two of the more rigid proline residues (P105 and P111) to alanines in the tether of HSO to study the effects of increased flexibility on the IET kinetics. We also made the double mutant P105A/P111A. The P105 residue is found at the N-terminal end of the tether, next to the heme, and P111 is found at the center of the tether. While P105 is conserved within cSO and HSO, P111 is not. However, P111 is conserved within other mammalian forms. Figure 2 illustrates the dependence of k_{et} on pH and mutation. The data show that the P105A mutation decreases k_{et} by approximately 3-fold (467 ± 19 s^{-1} at pH 7.4 for *wt* vs 146 ± 23 s^{-1} for P105A). In contrast, the P111A mutation has an only minimal effect on k_{et}. The IET rate constants for the P105A/P111A double mutant are similar to those for P105A, suggesting that the P105A change is the primary cause of the decrease in the IET rate constant that is observed in this mutant.

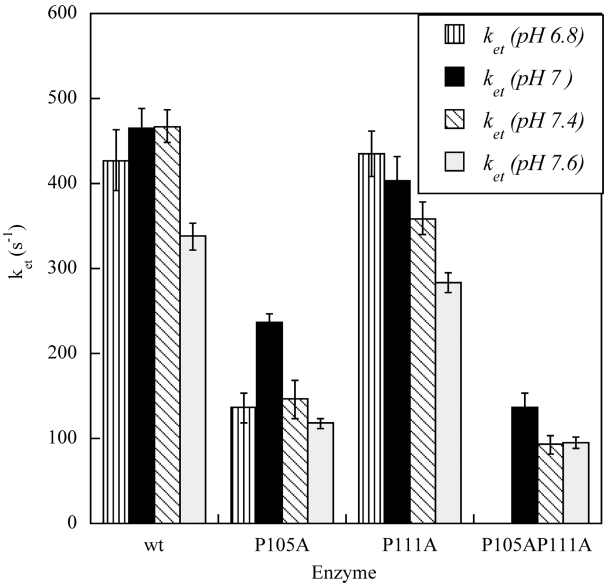

FIGURE 2: IET rate constants for the proline to alanine tether mutants.

Table 1: Laser Flash Photolysis Equilibrium Constants for Proline to Alanine Tether Mutants

	pH 6.8	pH 7.0	pH 7.4	pH 7.6
wt HSO	0.26 ± 0.01	0.35 ± 0.01	0.46 ± 0.02	0.45 ± 0.02
P105A	0.22 ± 0.01	0.38 ± 0.02	0.19 ± 0.02	0.44 ± 0.03
P111A	0.28 ± 0.02	0.36 ± 0.01	0.43 ± 0.01	0.44 ± 0.02
P105A/P111A	ND[a]	0.19 ± 0.01	0.33 ± 0.02	0.34 ± 0.01

[a]No heme reoxidation was observed.

The equilibrium constants (K_{eq}) for these mutants at various pH values are given in Table 1. For *wt* HSO, K_{eq} increases with an increase in pH. This trend is also observed for the P111A mutant, but not for the P105A and P105A/P111A mutants. However, the pH dependence of K_{eq} for the P105A and P105A/P111A mutants is similar. From the kinetic analysis of IET in these P to A mutants, we infer that mutation of P111, which is in the middle of the tether and not conserved across species, has little effect on the IET kinetics. However, the large decrease in IET kinetics for P105A suggests that this conserved proline, which is adjacent to the heme domain, promotes a tether conformation that results in optimal IET.

Steady-State Kinetics of Proline to Alanine Mutations. The steady-state oxidation of sulfite to sulfate as catalyzed

Table 2: Steady-State Kinetic Data for Proline to Alanine Tether Mutants[a]

enzyme	k_{cat} (s^{-1})	$K_m^{sulfite}$ (μM)	$k_{cat}/K_m^{sulfite}$ (M^{-1} s^{-1})
wt HSO[b]	26.9 ± 0.5	11.1 ± 0.4	2.4×10^6
P105A	39 ± 2	6 ± 1	6.1×10^6
P111A	50 ± 3	33 ± 5	1.5×10^6
P105A/P111A	46 ± 2	32 ± 3	1.5×10^6

[a]At pH 8.0 with 20 mM Tris acetate. [b]From refs *14* and *15*.

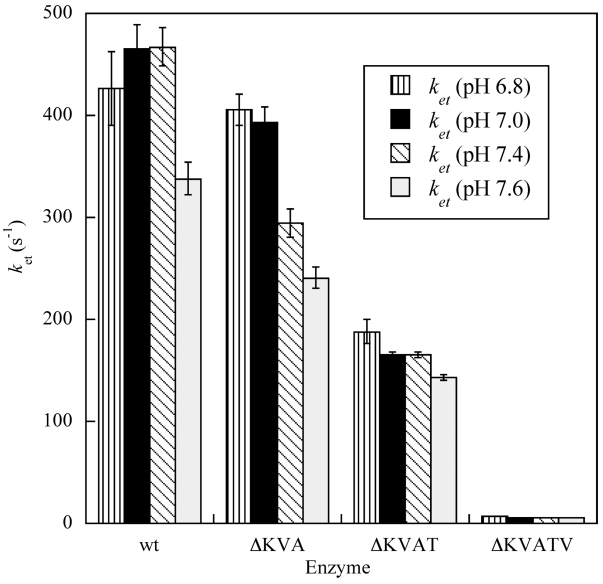

FIGURE 3: IET rate constants for tether deletion mutants.

by HSO using cyt *c* as the electron acceptor yields plots of initial velocity versus substrate concentration that display typical saturation kinetics (not shown). The standard Michaelis–Menten parameters at pH 8.0 are listed in Table 2. The largest effect observed is on the Michaelis–Menten constants (K_m) for P111A and P105A/P111A, which are approximately 5-fold higher than for *wt*. This increase in K_m also affects the catalytic efficiency (k_{cat}/K_m) of the enzyme, causing a 30% decrease in this parameter. From these results, we conclude that the P111A mutation may affect the binding of sulfite to the enzyme. Also, the steady-state data reveal that the k_{cat} values for each of these mutations are much smaller than k_{et}. Therefore, the IET process is not rate-limiting in catalysis, as is also true of the *wt* enzyme.

Laser Flash Photolysis Kinetics of Deletion Mutants. Deletions of nonconserved amino acids from the tether result in steadily decreasing IET rate constants, from 467 ± 19 s^{-1} in *wt* HSO to 5.59 ± 0.03 s^{-1} in ΔKVATV HSO (see Materials and Methods for abbreviations of deletion mutants) at pH 7.4 (Figure 3). Interestingly, the largest decrease occurs on deletion of the fifth residue. Additionally, all three deletion mutants exhibit decreasing IET rates with an increase in pH from 6.8 to 7.6. K_{eq} is significantly larger for ΔKVATV HSO [0.91 ± 0.03 (Table 3)] in comparison to the *wt* HSO value (0.46 ± 0.02) and those of the other tether deletion mutants, but all the enzymes seem to have a maximal K_{eq} around pH 7.4. The large increase in K_{eq} for ΔKVATV could be the result of changes in the potential of the molybdenum or heme centers. To test this possibility, we have also performed spectroelectrochemistry studies on *wt* and ΔKVATV HSO (see below).

Steady-State Kinetics of Deletion Mutations. Table 4 gives the steady-state data for the deletion mutants. Whereas the

Table 3: Laser Flash Photolysis Equilibrium Constants for Tether Deletion Mutants

	pH 6.8	pH 7.0	pH 7.4	pH 7.6
wt HSO	0.26 ± 0.01	0.35 ± 0.01	0.46 ± 0.02	0.45 ± 0.02
ΔKVA	0.36 ± 0.01	0.35 ± 0.01	0.50 ± 0.02	0.54 ± 0.02
ΔKVAT	0.41 ± 0.02	0.35 ± 0.03	0.56 ± 0.01	0.53 ± 0.03
ΔKVATV	0.59 ± 0.01	0.63 ± 0.02	0.91 ± 0.03	0.87 ± 0.03

Table 4: Steady-State Kinetic Data for Tether Deletion Mutants[a]

enzyme	k_{cat} (s^{-1})	$K_m^{sulfite}$ (μM)	$k_{cat}/K_m^{sulfite}$ (M^{-1} s^{-1})
wt HSO[b]	27 ± 1	11.1 ± 0.4	2.4×10^6
ΔKVA	40 ± 2	42 ± 4	9.5×10^5
ΔKVAT	35 ± 2	26 ± 2	1.4×10^6
ΔKVATV	10.6 ± 0.3	2.6 ± 0.4	4.1×10^6

[a]At pH 8.0 with 20 mM Tris acetate. [b]From refs *14* and *15*.

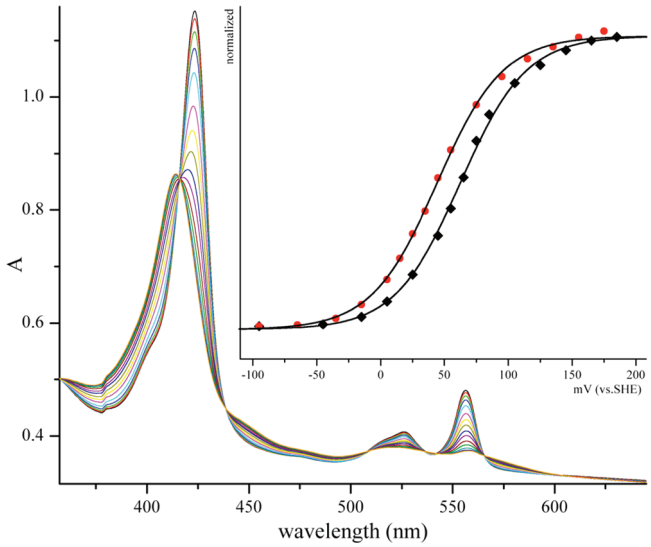

FIGURE 4: Spectroelectrochemical titration of the b_5 heme of wild-type HSO at pH 7.5 and 27 °C. The inset shows the fit of the data to eq 11 at 413 nm (*53*) (black for *wt* and red for ΔKVATV).

catalytic turnover numbers for the first two deletion mutants, ΔKVA and ΔKVAT HSO, are slightly increased in comparison to that of the *wt* enzyme, the turnover number for ΔKVATV HSO (10.6 ± 0.3 s^{-1}) is approximately one-third of that of *wt* (26.9 ± 0.5) at pH 8.0. $K_m^{sulfite}$ follows a similar trend, although it increases 4-fold for ΔKVA HSO in comparison to that of *wt* and decreases dramatically in ΔKVATV. In addition, $K_M^{cyt\ c}$ is larger for all of the deletion mutants (data not shown). Note that the turnover number for the ΔKVATV mutant is approximately the same as the IET rate constant for this mutant (see above). This suggests that for ΔKVATV, IET has become rate-limiting for catalysis.

Electrochemistry. As noted above, the laser flash photolysis data for ΔKVATV resulted in K_{eq} values that were approximately 0.91, compared to 0.46 for the *wt*. Consequently, the midpoint potential difference between the heme and molybdenum must have changed in this mutant. To confirm this, we have performed spectroelectrochemistry studies to determine the Fe(III/II) potentials for *wt* and ΔKVATV HSO. The corresponding midpoint potentials versus the SHE are 62 ± 2 mV for *wt* HSO and 44 ± 2 mV for ΔKVATV HSO (Figure 4 and Table 5). Thus, the Fe(III/II) potential for ΔKVATV HSO is 18 ± 3 mV

Table 5: Electrochemical Midpoint Potentials of HSO Cofactors[a]

cofactor	*wt*	ΔKVATV	P105A
$\Delta E^0_{\text{reaction (Heme-Mo)}}$[b]	19.94 ± 0.04	2.42 ± 0.03	20.05 ± 0.04
heme [Fe(III/II)][c]	62 ± 2	42 ± 2	56 ± 3
molybdenum(VI/V)[d]	42 ± 2	41 ± 1	36 ± 1

[a]All potentials are in millivolts vs the SHE. [b]Calculated from the equilibrium constants in Table 3 and the relationship $nF\Delta E^0 = -RT \ln K_{eq}$. [c]Determined by spectroelectrochemistry (see Figure 4). [d]Calculated from $\Delta E^0_{\text{reaction (Heme-Mo)}}$ and the experimental heme potential.

more negative than that of *wt*, supporting the laser flash photolysis kinetic data and favoring the Fe(III)/Mo(V) species in eq 5. Using the K_{eq} value from the laser flash photolysis data and the heme potential, the potential of the molybdenum center can be calculated as well. The calculated potentials of the Mo(VI)/Mo(V) couple for ΔKVATV and *wt* HSO are 41 ± 2 and 42 ± 2 mV, respectively (Table 5). Therefore, we conclude that the change in K_{eq} for ΔKVATV is primarily due to a change in the potential of the heme. Perhaps the deletion of five amino acids from the tether changes the exposure of the heme to solvent, thereby causing a shift in the potential and in K_{eq}.

We have also used spectroelectrochemistry to measure the Fe(III/II) potential of the P105A mutant which shows much slower rates of IET compared to that of *wt* but similar K_{eq} values (Figure 2 and Table 1). Table 5 shows that the Fe(III/II) potential for P105A is essentially identical to that of *wt*, as is the calculated Mo(VI/V) potential. Thus, the P105A mutation does not change the thermodynamic driving force for IET (as seen from K_{eq}) or the individual potentials of the two redox centers. Therefore, we conclude that the 2−4-fold decrease in k_{et} for P105A compared to *wt* (Figure 2) reflects differences in their IET pathways.

Electron Paramagnetic Resonance Spectra. The CW EPR spectra of all of the tether variants of HSO were essentially identical to that of *wt* HSO. Together with the similarity in potentials of the Mo centers (see above), the EPR spectra indicate that no changes in the Mo environment were caused by the tether deletions or P → A mutations. Specifically, at pH 5.8 in the presence of 100 mM chloride, the low-pH (*lpH*) form of the Mo(V) center was generated, characterized by principal *g* values of 2.004, 1.973, and 1.966 with proton hyperfine splittings of 0.8, 0.6, and 1.2 mT at the EPR turning points (*60*, *61*). At pH 9, the so-called high-pH (*hpH*) form of the Mo(V) center was obtained, characterized by principal *g* values of 1.988, 1.964, and 1.953 (*60*, *61*).

CONCLUSION

This work presents the first experimental investigation of the kinetic effects of altering the nature of the tether connecting the heme and molybdenum domains of HSO. Changing the flexibility of the tether has been explored by replacing two prolines with alanines. The P105A substitution, which is adjacent to the heme domain and presumably would increase tether flexibility, leads to a marked decrease in IET rates, whereas the P111A substitution in the center of the tether has little effect on the IET kinetics. These observations suggest that no generalizations can be made regarding the kinetic effect of flexibility, and that the rigidity of P105 may favor a tether conformation that results in more facile IET. This is presumably a consequence of a more favorable orientation between the heme and the Mo centers during the electron transfer process. We conclude that these results do not provide support for a role of tether flexibility in causing the faster IET rate in chicken versus human SO.

Deletion of amino acids from the tether resulted in pronounced decreases in IET rates. For the ΔKVATV deletion, IET became rate-limiting. Decreasing the length of the tether can influence the docking of the heme domain onto the molybdenum domain, thereby changing the distance and relative orientation of the two redox centers. This is the probable reason for the decrease in k_{et}. In addition, shortening the tether by five amino acids decreased the Fe(III/II) potential of the b_5 heme center by 20 mV without affecting the molybdenum potential (Table 5). The similarity of the EPR spectra of all of the variants to that of *wt* HSO further indicates that the geometry of the molybdenum active site remains unchanged. The small change in the Fe(III/II) potential could be due to increased exposure of the heme to solvent in this variant and translates to a decrease in the driving force (ΔG^0) for reaction 5 of only ~2 kJ/mol. It seems unlikely that such a relatively small change in the driving force could account for the 70-fold decrease in k_{et} observed in the ΔKVATV deletion mutant. The reorganization energy of this mutant is expected to differ little from that of *wt*, and previous studies of the relationship between k_{et} and ΔG^0 in the amicyanin−cytochrome c_{551i} mutant system showed that a 145-fold decrease in k_{et} involved a decrease in driving force of 19 kJ/mol (*62*), 10 times larger than that found in this work.

We conclude that the results presented here point to a critical role of the tether in facilitating the IET reaction between the heme and molybdenum centers. This supports the contention that a conformational transition is required to bring these two centers into a suitable mutual orientation (*17*). While "simple docking" within a narrow range of orientations is a reasonable conclusion for SO, the new "dynamic docking" paradigm for protein−protein complexes proposed by Hoffman and co-workers from recent studies on Zn-myoglobin and cytochrome b_5 must also be considered (*63*). A key feature of this paradigm is the presence of numerous weakly bound conformations, some of which greatly facilitate electron transfer (*63*). Thus, for SO, it is possible that k_{et} is the result of many averaged conformations of SO, as well as the overall driving force and reorganization energy (*62*). Finally, this study provides experimental data for testing computational models for electron transfer in a two-domain enzyme (*45*). However, such calculations are beyond the scope of this work.

ACKNOWLEDGMENT

We are indebted to Professor K. V. Rajagopalan for providing the pTG918 plasmid containing the HSO gene for preparing recombinant human sulfite oxidase and the protocols for purifying the enzyme. We are grateful to Professor F. Ann Walker for the use of equipment and for helpful discussions. We thank Drs. Heather Wilson, John Yang, and Arnold Raitsimring for helpful discussions.

SUPPORTING INFORMATION AVAILABLE

Primer design; iron to molybdenum ratios determined using inductively coupled plasma; and laser flash photolysis results for proline to alanine and deletion mutants. This material is available free of charge via the Internet at http://pubs.acs.org.

REFERENCES

1. Hille, R. (1996) The Mononuclear Molybdenum Enzymes. *Chem. Rev. 96*, 2757–2816.
2. Rajagopalan, K. V., and Johnson, J. L. (2002) Sulfite Oxidase. In Wiley Encyclopedia of Molecular Medicine (Creighton, T. E., Ed.) pp 3048−3051, Wiley, New York.

3. Kisker, C. (2001) Sulfite Oxidase. In Handbook of Metalloproteins (Messerschmidt, A., Huber, R., Poulos, T., and Wieghardt, K., Eds.) pp 1121−1135, John Wiley and Sons, Ltd., New York.
4. Schindelin, H., Kisker, C., and Rajagopalan, K. V. (2001) Molybdopterin from molybdenum and tungsten enzymes. *Adv. Protein Chem. 58*, 47–94.
5. Cohen, H. J., Betcher-Lange, S., Kessler, D. L., and Rajagopalan, K. V. (1972) Hepatic Sulfite Oxidase. Congruency in mitochondria of prosthetic groups and activity. *J. Biol. Chem. 247*, 7759–7766.
6. Kessler, D. L., Johnson, J. L., Cohen, H. J., and Rajagopalan, K. V. (1974) Visualization of Hepatic Sulfite Oxidase in Crude Tissue Preparations by Electron Paramagnetic Resonance Spectroscopy. *Biochim. Biophys. Acta 334*, 86–96.
7. Sullivan, E. P., Jr., Hazzard, J. T., Tollin, G., and Enemark, J. H. (1993) Electron Transfer in Sulfite oxidase: Effects of pH and anions on transient kinetics. *Biochemistry 32*, 12465–12470.
8. Brody, M. S., and Hille, R. (1999) The kinetic behavior of chicken liver sulfite oxidase. *Biochemistry 38*, 6668–6677.
9. Kessler, D. L., and Rajagopalan, K. V. (1972) Purification and properties of sulfite oxidase from chicken liver. Presence of molybdenum in sulfite oxidase from diverse sources. *J. Biol. Chem. 247*, 6566–6573.
10. Garrett, R. M., and Rajagopalan, K. V. (1994) Molecular cloning of rat liver sulfite oxidase. Expression of a eukaryotic Mo-pterin-containing enzyme in *Escherichia coli*. *J. Biol. Chem. 269*, 272–276.
11. Feng, C., Wilson, H. L., Hurley, J. K., Hazzard, J. T., Tollin, G., Rajagopalan, K. V., and Enemark, J. H. (2003) Role of Conserved Tyrosine 343 in Intramolecular Electron Transfer in Human Sulfite Oxidase. *J. Biol. Chem. 278*, 2913–2920.
12. Feng, C., Wilson, H. L., Hurley, J. K., Hazzard, J. T., Tollin, G., Rajagopalan, K. V., and Enemark, J. H. (2003) Essential role of conserved arginine 160 in intramolecular electron transfer in human sulfite oxidase. *Biochemistry 42*, 12235–12242.
13. Feng, C., Wilson, H. L., Tollin, G., Astashkin, A. V., Hazzard, J. T., Rajagopalan, K. V., and Enemark, J. H. (2005) The pathogenic human sulfite oxidase mutants G473D and A208D are defective in intramolecular electron transfer. *Biochemistry 44*, 13734–13743.
14. Wilson, H. L., and Rajagopalan, K. V. (2004) The role of tyrosine 343 in substrate binding and catalysis by human sulfite oxidase. *J. Biol. Chem. 279*, 15105–15113.
15. Wilson, H. L., Wilkinson, S. R., and Rajagopalan, K. V. (2006) The G473D mutation impairs dimerization and catalysis in human sulfite oxidase. *Biochemistry 45*, 2149–2160.
16. Kisker, C., Schindelin, H., Pacheco, A., Wehbi, W. A., Garrett, R. M., Rajagopalan, K. V., Enemark, J. H., and Rees, D. C. (1997) Molecular basis of sulfite oxidase deficiency from the structure of sulfite oxidase. *Cell 91*, 973–983.
17. Feng, C., Kedia, R. V., Hazzard, J. T., Hurley, J. K., Tollin, G., and Enemark, J. H. (2002) Effect of Solution Viscosity on Intramolecular Electron Transfer in Sulfite Oxidase. *Biochemistry 41*, 5816–5821.
18. Winkler, J. R., Nocera, D. G., Yocom, K. M., Bordignon, E., and Gray, H. B. (1982) Electron-transfer kinetics of pentaammineruthenium(III)(histidine-33)-ferricytochrome *c*. Measurement of the rate of intramolecular electron transfer between redox centers separated by 15 Å in a protein. *J. Am. Chem. Soc. 104*, 5798–5800.
19. Moser, C. C., Keske, J. M., Warncke, K., Farid, R. S., and Dutton, P. L. (1992) Nature of biological electron transfer. *Nature 355*, 796–802.
20. Pasman, P., Koper, N. W., and Verhoeven, J. W. (1982) Photoinduced long-range electron transfer in rigid bichromophoric molecules. *Recl. Trav. Chim. Pays-Bas 101*, 363–364.
21. Calcaterra, L. T., Closs, G. L., and Miller, J. R. (1983) Intramolecular electron transfer in radical ions over long distances across rigid saturated hydrocarbon spacers. *J. Am. Chem. Soc. 105*, 670–671.
22. Freed, K. F. (1983) Role of intramolecular vibrational relaxation on electron transfer rates: Application to pentaammineruthenium(III) (histidine-33)-ferrcytochrome *c*. *Chem. Phys. Lett. 97*, 489–493.
23. McGourty, J. L., Blough, N. V., and Hoffman, B. M. (1983) Electron transfer at crystallographically known long distances (25 Å) in [Zn(II), Fe(III)] hybrid hemoglobin. *J. Am. Chem. Soc. 105*, 4470–4472.
24. Overfield, R. E., Scherz, A., Kaufmann, K. J., and Wasielewski, M. R. (1983) Photoinduced electron-transfer reactions in a chlorophyllide-pheophorbide cyclophane. A model for photosynthetic reaction centers. *J. Am. Chem. Soc. 105*, 5747–5752.
25. Simolo, K. P., McLendon, G. L., Mauk, M. R., and Mauk, A. G. (1984) Photoinduced electron transfer within a protein-protein complex formed between physiological redox partners-reduction of ferricytochrome b_5 by the hemoglobin derivative α_2Zn-$\beta_2Fe^{III}(CN)$. *J. Am. Chem. Soc. 106*, 5012–5013.
26. Gunner, M. R., Robertson, D. E., and Dutton, P. L. (1986) Kinetic studies on the reaction center protein from *Rhodopseudomonas sphaeroides*: The temperature and free-energy dependence of electron transfer between various quinones in the QA site and the oxidized bacteriochlorophyll dimer. *J. Phys. Chem. 90*, 3783–3795.
27. Heitele, H., Michel-Beyerle, M. E., and Finckh, P. (1987) Electron transfer through intramolecular bridges in donor/acceptor systems. *Chem. Phys. Lett. 134*, 273–278.
28. Closs, G. L., and Miller, J. R. (1988) Intramolecular long-distance electron transfer in organic molecules. *Science 240*, 440–447.
29. Kuki, A., and Wolynes, P. G. (1987) Electron tunneling paths in proteins. *Science 236*, 1647–1652.
30. Lawson, J. M., Craig, D. C., Paddon-Row, M. N., Kroon, J., and Verhoeven, J. W. (1989) Through-bond modulation of intramolecular electron transfer in rigidly linked donor-acceptor systems. *Chem. Phys. Lett. 164*, 120–125.
31. Evenson, J. W., and Karplus, M. (1993) Effective coupling in biological electron transfer: Exponential or complex distance dependence. *Science 262*, 1247–1249.
32. Gray, H. B., and Winkler, J. R. (1996) Electron transfer in proteins. *Annu. Rev. Biochem. 65*, 537–561.
33. Kuzetsov, A. M., and Ulstrup, J. (1998) Electron Transfer in Chemistry and Biology: An Introduction to the Theory, John Wiley and Sons, Inc., Hoboken, NJ.
34. Skourtis, S. S., and Beratan, D. N. (1998) Electron transfer mechanisms. *Curr. Opin. Chem. Biol. 2*, 235–243.
35. Verhoeven, J. W. (1999) From close contact to long-range intramolecular electron transfer. *Adv. Chem. Phys. 106*, 603–644.
36. Winkler, J. R. (2000) Electron tunneling pathways in proteins. *Curr. Opin. Chem. Biol. 4*, 192–198.
37. Gray, H. B., and Winkler, J. R., Eds. (2003) Heme protein dynamics: Electron tunneling and redox triggered folding. In The Porphyrin Handbook: Bioinorganic and Bioorganic Chemistry, Vol. *11*, Academic Press, San Diego.
38. Gray, H. B., and Winkler, J. R. (2001) Electron transfer in biological systems. In Electron Transfer in Chemistry, (Balzani, V., Ed.) Vol. *III*, pp 1−175, Wiley-VCH, Weinheim, Germany.
39. Paddon-Row, M. N. (2003) Superexchange-mediated charge separation and charge recombination in covalently linked donor-bridge-acceptor systems. *Aust. J. Chem. 56*, 729–748.
40. Hopfield, J. J. (1974) Electron Transfer Between Biological Molecules by Thermally Activated Tunneling. *Proc. Natl. Acad. Sci. U.S.A. 71*, 3640–3644.
41. Beratan, D. N., Betts, J. N., and Onuchic, J. N. (1991) Protein Electron Transfer Rates Set by the Bridging Secondary and Tertiary Structure. *Science 252*, 1285–1288.
42. Gray, H. B., and Winkler, J. R. (2003) Electron tunneling through proteins. *Q. Rev. Biophys. 36*, 341–372.
43. Winkler, J. R., Wittung-Stafshede, P., Lekner, J., Malmstrom, B. G., and Gray, H. B. (1997) Effects of folding on metalloprotein active sites. *Proc. Natl. Acad. Sci. U.S.A. 94*, 4246–4249.
44. Feng, C., Tollin, G., and Enemark, J. H. (2007) Sulfite oxidizing enzymes. *Biochim. Biophys. Acta 1774*, 527–539.
45. Kawatsu, T., and Beratan, D. N. (2006) Electron transfer between cofactors in protein domains linked by a flexible tether. *Chem. Phys. 326*, 259–269.
46. Temple, C. A., Graf, T. N., and Rajagopalan, K. V. (2000) Optimization of expression of human sulfite oxidase and its molybdenum domain. *Arch. Biochem. Biophys. 383*, 281–287.
47. Garrett, R. M., and Rajagopalan, K. V. (1996) Site-directed mutagenesis of recombinant sulfite oxidase: Identification of cysteine 207 as a ligand of molybdenum. *J. Biol. Chem. 271*, 7387–7391.
48. Pacheco, A., Hazzard, J. T., Tollin, G., and Enemark, J. H. (1999) The pH dependence of intramolecular electron transfer rates in sulfite oxidase at high and low anion concentrations. *J. Biol. Inorg. Chem. 4*, 390–401.
49. Hurley, J. K., Weber-Main, A. M., Stankovich, M. T., Benning, M. M., Thoden, J. B., Vanhooke, J. L., Holden, H. M., Chae, Y. K., Xia, B., Cheng, H., Markley, J. L., Martinez-Julvez, M., Gomez-Moreno, C., Schmetis, J. L., and Tollin, G. (1997) Structure-Function Relationships in *Anabaena* Ferredoxin: Correlations between X-ray Crystal Structures, Reduction Potentials, and Rate Constants of Electron Transfer to Ferredoxin:$NADP^+$ Reductase for Site-Specific Ferredoxin Mutants. *Biochemistry 36*, 11100–11117.
50. Tollin, G., Hurley, J. K., Hazzard, J. T., and Meyer, T. E. (1993) Use of laser flash photolysis time-resolved spectrophotometry to investigate interprotein and intraprotein electron transfer mechanisms. *Biophys. Chem. 48*, 259–279.

51. Tollin, G. (1995) Use of flavin photochemistry to probe intra-protein and interprotein electron transfer mechanisms. *J. Bioenerg. Biomembr. 27*, 303–309.
52. Tollin, G. (2001) Interprotein and Intraprotein Electron Transfer Mechanisms. In Electron Transfer in Chemistry (Balzani, V., Ed.) Vol. *IV*, pp 202−231, Wiley-VCH: Weinheim, Germany.
53. Ding, X. D., Weichsel, A., Andersen, J. F., Shokhireva, T. Kh., Balfour, C., Pierik, A. J., Averill, B. A., Montfort, W. R., and Walker, F. A. (1999) Nitric Oxide Binding to the Ferri- and Ferroheme States of Nitrophorin 1, a Reversible NO-Binding Heme Protein from the Saliva of the Blood-Sucking Insect, *Rhodnius prolixus*. *J. Am. Chem. Soc. 121*, 128–138.
54. Berry, R. E., Shokhireva, T. Kh., Filippov, I., Shokhirev, M. N., Zhang, H., and Walker, F. A. (2007) Effect of the N-Terminus on Heme Cavity Structure, Ligand Equilibrium, Rate Constants, and Reduction Potentials of Nitrophorin 2 from *Rhodnius prolixus*. *Biochemistry 46*, 6830–6843.
55. Hellwig, P., Bwhr, J., Ostermeier, C., Oliver-Matthias, H. R., Pfitzner, U., Odenwald, A., Ludwig, B., Hartmut, M., and Mantele, W. (1998) Involvement of Glutamic Acid 278 in the Redox Reaction of the Cytochrome *c* Oxidase from *Paracoccus denitrificans* Investigated by FTIR Spectroscopy. *Biochemistry 37*, 7390–7399.
56. Klein, E. L., Astashkin, A. V., Ganyushin, D., Riplinger, C., Johnson-Winters, K., Neese, F., and Enemark, J. H. (2009) Direct Detection and Characterization of Chloride in the Active Site of the Low-pH Form of Sulfite Oxidase Using Electron Spin Echo Envelope Modulation Spectroscopy, Isotopic Labeling, and Density Functional Theory Calculations. *Inorg. Chem. 48*, 4743–4752.
57. Astashkin, A. V., Johnson-Winters, K., Klein, E. L., Byrne, R. S., Hille, R., Raitsimring, A. M., and Enemark, J. H. (2007) Direct demonstration of the presence of coordinated sulfate in the reaction pathway of *Arabidopsis thaliana* sulfite oxidase using ^{33}S labeling and ESEEM spectroscopy. *J. Am. Chem. Soc. 129*, 14800–14810.
58. Astashkin, A. V., Johnson-Winters, K., Klein, E. L., Feng, C., Wilson, H. L., Rajagopalan, K. V., Raitsimring, A. M., and Enemark, J. H. (2008) Structural studies of the molybdenum center of the pathogenic R160Q mutant of human sulfite oxidase by pulsed EPR spectroscopy and ^{17}O and ^{33}S labeling. *J. Am. Chem. Soc. 130*, 8471–8480.
59. Astashkin, A. V., Hood, B. L., Feng, C., Hille, R., Mendel, R. R., Raitsimring, A. M., and Enemark, J. H. (2005) Structures of the Mo(V) forms of sulfite oxidase from *Arabidopsis thaliana* by pulsed EPR spectroscopy. *Biochemistry 44*, 13274–13281.
60. Lamy, M. T., Gutteridge, S., and Bray, R. C. (1980) Electron-paramagnetic-resonance parameters of molybdenum(V) in sulphite oxidase from chicken liver. *Biochem. J. 185*, 397–403.
61. Enemark, J. H., Astashkin, A. V., and Raitsimring, A. M. (2006) Investigation of the coordination structures of the molybdenum(V) sites of sulfite oxidizing enzymes by pulsed EPR spectroscopy. *Dalton Trans.,* 3501–3514.
62. Davidson, V. L. (2008) Protein Control of True, Gated, and Coupled Electron Transfer Reactions. *Acc. Chem. Res. 41*, 730–738.
63. Liang, Z., Nocek, J. M., Huang, K., Hayes, R. T., Kurnikov, I. V., Beratan, D. N., and Hoffman, B. M. (2002) Dynamic Docking and Electron Transfer between Zn-myoglobin and Cytochrome b_5. *J. Am. Chem. Soc. 124*, 6849–6859.